








# New Insights into the Nature of Turbulence in the Earth's Magnetosheath Using Magnetospheric MultiScale Mission Data

H. Breuillard<sup>1</sup>, L. Matteini<sup>2</sup> , M. R. Argall<sup>3</sup> , F. Sahraoui<sup>1</sup>, M. Andriopoulou<sup>4</sup>, O. Le Contel<sup>1</sup>, A. Retinò<sup>1</sup>, L. Mirioni<sup>1</sup>, S. Y. Huang<sup>5</sup>, D. J. Gershman<sup>6</sup>, R. E. Ergun<sup>7</sup>, F. D. Wilder<sup>7</sup>, K. A. Goodrich<sup>7</sup>, N. Ahmadi<sup>7</sup>, E. Yordanova<sup>8</sup>, A. Vaivads<sup>8</sup> , D. L. Turner<sup>9</sup>, Yu. V. Khotyaintsev<sup>8</sup> , D. B. Graham<sup>8</sup>, P.-A. Lindqvist<sup>10</sup>, A. Chasapis<sup>11</sup> , J. L. Burch<sup>12</sup>, R. B. Torbert<sup>3</sup>, C. T. Russell<sup>13</sup>, W. Magnes<sup>4</sup>, R. J. Strangeway<sup>13</sup>, F. Plaschke<sup>4</sup>, T. E. Moore<sup>6</sup>, B. L. Giles<sup>6</sup>, W. R. Paterson<sup>6</sup>, C. J. Pollock<sup>6</sup>, B. Lavraud<sup>14</sup>, S. A. Fuselier<sup>12</sup>, and I. J. Cohen<sup>15</sup>

<sup>1</sup> Laboratoire de Physique des Plasmas, UMR7648, CNRS/Ecole Polytechnique/Sorbonne Univ./Univ. Paris Sud, Paris, France; [hbreuill@gmail.com](mailto:hbreuill@gmail.com)

<sup>2</sup> LESIA-Observatoire de Paris/PSL Research University/CNRS/UPMC Université Paris 06/Université Paris-Diderot, Meudon, France

<sup>3</sup> University of New Hampshire, Durham, NH, USA

<sup>4</sup> Space Research Institute, Austrian Academy of Sciences, Graz, Austria

<sup>5</sup> School of Electronics and Information, Wuhan University, Beijing, People's Republic of China

<sup>6</sup> NASA Goddard Space Flight Center, Greenbelt, MD, USA

<sup>7</sup> University of Colorado, Laboratory for Atmospheric and Space Physics, Boulder, CO, USA

<sup>8</sup> Swedish Institute of Space Physics, Uppsala, Sweden

<sup>9</sup> Space Sciences Department, The Aerospace Corporation, El Segundo, CA, USA

<sup>10</sup> Royal Institute of Technology, Stockholm, Sweden

<sup>11</sup> University of Delaware, Newark, DE, USA

<sup>12</sup> Southwest Research Institute, San Antonio, TX, USA

<sup>13</sup> University of California, Los Angeles, CA, USA

<sup>14</sup> Institut de Recherche en Astrophysique et Planétologie (IRAP), CNRS UMR5277/Université Paul Sabatier, Toulouse, France

<sup>15</sup> Applied Physics Laboratory, The Johns Hopkins University, Laurel, MD, USA

Received 2018 January 23; revised 2018 March 14; accepted 2018 March 18; published 2018 May 30

## Abstract

The Earth's magnetosheath, which is characterized by highly turbulent fluctuations, is usually divided into two regions of different properties as a function of the angle between the interplanetary magnetic field and the shock normal. In this study, we make use of high-time resolution instruments on board the *Magnetospheric MultiScale* spacecraft to determine and compare the properties of subsolar magnetosheath turbulence in both regions, i.e., downstream of the quasi-parallel and quasi-perpendicular bow shocks. In particular, we take advantage of the unprecedented temporal resolution of the Fast Plasma Investigation instrument to show the density fluctuations down to sub-ion scales for the first time. We show that the nature of turbulence is highly compressible down to electron scales, particularly in the quasi-parallel magnetosheath. In this region, the magnetic turbulence also shows an inertial (Kolmogorov-like) range, indicating that the fluctuations are not formed locally, in contrast with the quasi-perpendicular magnetosheath. We also show that the electromagnetic turbulence is dominated by electric fluctuations at sub-ion scales ( $f > 1$  Hz) and that magnetic and electric spectra steepen at the largest-electron scale. The latter indicates a change in the nature of turbulence at electron scales. Finally, we show that the electric fluctuations around the electron gyrofrequency are mostly parallel in the quasi-perpendicular magnetosheath, where intense whistlers are observed. This result suggests that energy dissipation, plasma heating, and acceleration might be driven by intense electrostatic parallel structures/waves, which can be linked to whistler waves.

**Key words:** acceleration of particles – Earth – planets and satellites: magnetic fields – plasmas – turbulence – waves

## 1. Introduction

The Earth's magnetosheath (MSH) constitutes the interface between the streaming solar wind and the standing magnetosphere. It forms as the solar wind plasma decelerates and heats at the terrestrial bow shock and flows along the frontier of the Earth's magnetosphere, i.e., the magnetopause (MP). The magnetosheath is usually divided into two distinct regions: (i) the quasi-parallel magnetosheath located downstream of the quasi-parallel shock, i.e., where the angle  $\theta_{Bn}$  between the shock normal and the upstream interplanetary magnetic field is less than  $45^\circ$ , and (ii) the quasi-perpendicular magnetosheath, where  $\theta_{Bn} > 45^\circ$ . This distinction is due to the fact that the structure, dynamics, and dissipation processes of the bow shock vary considerably, depending on the angle  $\theta_{Bn}$  but also on the plasma  $\beta$  (the ratio of plasma to magnetic pressure in the upstream region).

In the foreshock upstream of the quasi-parallel bow shock, the power of the magnetic fluctuations is roughly one order of magnitude larger than that upstream of the quasi-perpendicular shock (Czaykowska et al. 2001). This is due to ions reflected at the quasi-parallel shock that can drive ion beam instabilities (Sckopke et al. 1983; Thomsen et al. 1985) that excite large-amplitude waves (Le & Russell 1992). The amplification of convecting upstream waves and the wave generation at the shock interface probably enhance the magnetic power by a factor of four at the shock itself, whereas there is no significant difference in the magnetic power spectra upstream of and downstream of the quasi-parallel bow shock (Czaykowska et al. 2001).

In contrast, at quasi-perpendicular shocks, the reflected ions gyrate back to the shock and enter the downstream region, where the magnetic wave activity is considerably higher than the upstream. In fact, the presence of these ions generates a

high perpendicular-temperature anisotropy  $T_{\perp i} > T_{\parallel i}$  ( $\parallel$  and  $\perp$  to the magnetic field; Scokpe et al. 1983), causing various local fluid and kinetic instabilities that lead to the generation of a rich variety of waves (ion-cyclotron waves, mirror modes, etc.) depending on the plasma  $\beta$ . These waves are commonly observed in the magnetosheath (see the review by Schwartz et al. 1996).

Downstream of the quasi-perpendicular, low- $\beta$  shock, a dominance of ion-cyclotron waves (left-hand polarized waves at frequencies just below the ion-cyclotron frequency,  $f_{ci}$ ) with amplitudes of about 3 nT is found, whereas mirror waves are mostly observed downstream of the quasi-perpendicular, high- $\beta$  shock (Russell & Farris 1995; Czaykowska et al. 2001). Due to the plasma flowing along the MP, a high-velocity shear is also observed in the magnetosheath, which is usually characterized by enhanced levels of turbulence (Zimbaro et al. 2010) that can interact with the present wave modes (see, e.g., Bale et al. 2009; Breuillard et al. 2016).

Turbulence is a natural way to convert the energy of large-scale motions into small-scale fluctuations. It is characterized by large and irregular fluctuations of the physical parameters (e.g., density, velocity, and electromagnetic field) from the largest (MHD) down to the smallest (electron) scales. In the incompressible MHD phenomenology, the energy cascades by nonlinear interactions among counter-propagating Alfvén wave packets to kinetic (ion and electron) scales, where it is eventually dissipated (see the review by Bruno & Carbone 2013). This fully developed turbulence is characterized by a spectrum of energy that follows a power law (Iroshnikov 1963; Kraichnan 1965). It is believed that at kinetic scales, turbulence plays a fundamental role in energy dissipation and plasma heating (Schekochihin et al. 2009). Therefore, it is crucial to characterize the properties of kinetic turbulence (e.g., scaling law, spectral anisotropy), the governing processes (e.g., wave-particle interactions), and the resulting coherent structures that can heat and accelerate electrons (see Zimbaro et al. 2010; Alexandrova et al. 2013; Franci et al. 2016, 2017; Huang et al. 2017b, 2017a, and references therein).

The ion and electron characteristic scales are defined as temporal scales, i.e., the ion and electron gyrofrequencies,  $f_{ci,e}$ , and spatial scales, namely the ion and electron gyroradii,  $f_{\rho_{i,e}}$ , and inertial lengths,  $f_{\lambda_{i,e}}$ . As the plasma bulk velocity in the solar wind is usually super-Alfvénic (i.e.,  $v_{\text{bulk}} \gg v_A$ ), spatial scales are usually transformed into temporal scales using Taylor’s hypothesis (Taylor 1938):  $f = v_{\text{bulk}}/(2\pi k)$ . Hence, high (low) frequencies correspond to small (large) spatial scales (wavenumbers) in the spectra.

However, Howes et al. (2014) and Klein et al. (2014) have shown that for  $\beta = 1$ , Taylor’s hypothesis can be violated under certain circumstances, such as the slow flow ( $v_{\text{bulk}} \lesssim v_A$ ) or the dispersive regime (e.g., in the case of parallel fast/whistler turbulence). In particular, Klein et al. (2014) showed that in the case of slow flow, the frequency spectrum is shifted toward higher frequencies, and in the case of whistler turbulence, this spectrum is significantly flattened for  $f/f_{ci} > 1$  but only when  $v_{\text{bulk}}/v_A \leq 3$ . Therefore, temporal frequencies observed by onboard spacecraft instruments could not be converted directly into spatial scales through that hypothesis for  $v_{\text{bulk}}/v_A \leq 1$  below ion gyrofrequency and for  $v_{\text{bulk}}/v_A \leq 3$  above it. In our case (i.e., in the magnetosheath),  $\beta \gg 1$  (see, e.g., Table 1); thus,  $v_{\text{ms}} > v_A$ , where  $v_{\text{ms}}$  is the magnetosonic speed. Hence, these waves are more likely to

violate the Taylor hypothesis here. We discuss below  $v_{\text{ms}}$ , along with  $v_A$  and  $v_{\text{bulk}}$ , for each case considered.

At MHD scales, i.e., below the ion-cyclotron frequency,  $f_{ci}$ , the power-law spectra,  $f^{-1.7}$  (Kolmogorov-like), which is typical of the solar wind inertial range, is usually observed far away from the bow shock in the flanks of the magnetosheath (Alexandrova et al. 2008; Huang et al. 2017), whereas an  $f^{-1}$  power-law spectrum is observed in the vicinity of the bow shock (Czaykowska et al. 2001). While magnetic-field variations in the foreshock are sometimes considered as probable sources of intensive variations in the magnetosheath (Fairfield & Ness 1970), Shevryev et al. (2006) have shown that the bow shock angle controls the properties of plasma turbulence in MSH. In particular, they observe a Kolmogorov-like spectrum, i.e., a developed turbulence, in the quasi-parallel MSH but not downstream of the quasi-perpendicular shock. However, the generation region of the turbulent fluctuations at MHD scales observed in the MSH remains unclear.

At kinetic scales, the energy of the magnetic fluctuations follows a power law close to  $f^{-2.8}$  (see, e.g., Alexandrova et al. 2008; Zimbaro et al. 2010; Matteini et al. 2017), as in the solar wind (see, e.g., Alexandrova et al. 2009, 2012). There two dominant wave modes have been suggested to be relevant, namely kinetic Alfvén waves (KAWs) and whistler waves (see, e.g., Chen et al. 2013, and references therein). However, the nonlinear equations that they are derived from have a similar form, and the turbulence energy spectra, obtained from dimensional arguments, are the same. Thus, a detailed polarization analysis of waveforms is required to identify the two wave modes. Another way to distinguish between KAWs and whistler waves in the solar wind was introduced in Chen et al. (2013). This technique is based on the difference between density fluctuations in the two different wave modes. In whistler turbulence, density fluctuations should be negligible ( $\delta \tilde{b}_{\perp} \gg \delta \tilde{n}$ ), whereas in KAWs,  $\delta \tilde{b}_{\perp} \approx \delta \tilde{n}$  is expected, where  $\delta \tilde{b}_{\perp}$  and  $\delta \tilde{n}$  are normalized density and perpendicular magnetic fluctuations in kinetic Alfvén turbulence (see, e.g., Schekochihin et al. 2009). While density fluctuations have been studied at large (MHD) scales in the solar wind (Chen et al. 2013) and in the magnetosheath (Sahraoui et al. 2006; Hadid et al. 2018), they have not been investigated at smaller (kinetic) scales, to our knowledge, due to instrumental limitations.

In this study, we take advantage of the high-time resolution instruments on board *Magnetospheric MultiScale (MMS)* to study the plasma turbulence from MHD to kinetic scales in Earth’s subsolar magnetosheath. In particular, the measurements are sampled at an unprecedented rate of 32 and 16 Hz for electron and ion velocity distribution functions, respectively, by the Fast Plasma Investigation (FPI; Pollock et al. 2016) instrument. The electric field and spacecraft potential are measured at a sampling frequency of 8192 Hz by the Electric-field Double Probe (EDP) instrument, which consists of the Axial Double Probe (Ergun et al. 2016) and the Spin Double Probe (Lindqvist et al. 2016) instruments. Low- and high-frequency magnetic-field measurements are sampled at a rate of 128 and 8192 Hz by the FluxGate Magnetometers (FGM; see Russell et al. 2016) and the search-coil magnetometer (SCM; see Le Contel et al. 2016) instruments, respectively. We investigate the nature of plasma turbulence, particularly density fluctuations—first at large (MHD) scale using survey-type measurements and then at small (kinetic) scale using burst-type data (for more details, see Fuselier et al. 2016)—in Earth’s

**Table 1**

Mean Spacecraft (MMS Position), Magnetosheath (Total Magnetic-field, Plasma Beta, Alfvén, and Fast Magnetosonic Speed) and Solar Wind<sup>a</sup> Parameters (Interplanetary Magnetic-field (IMF) Vector and Solar Wind Flow Pressure ( $p_{sw}$ )) Observed for the Four Cases Considered in this Study, and the Derived Angle between MP Normal and IMF ( $\theta_{Bn}$ ) Using the Shue et al. (1998) Model

Case	$[X, Y]_{GSE}$	IMF <sub>GSM</sub> (nT)	$p_{sw}$ (nPa)	$\theta_{Bn}$ (°)	$B_0$ (nT)	$\beta$	$v_A$ [km s <sup>-1</sup> ]	$v_{bulk}$ [km s <sup>-1</sup> ]	$v_{ms}$ [km s <sup>-1</sup> ]
1	[11.8, -0.2]	[0.02, -1.74, -3.06]	1.68	88	20	7.2	88	85	100
2	[11.7, -1.5]	[4.44, -1.1, -0.28]	2.35	18	25	6.9	100	200	130
3	[8, -5.5]	[-4.56, 0.92, 1.21]	5.59	13	25	13	40	130	60
4	[11, 1.2]	[1.36, -6.32, -7.86]	5.00	91	25	12	82	130	115

**Note.**

<sup>a</sup> Solar wind parameters are obtained from OMNIWEB (<https://omniweb.gsfc.nasa.gov>).

quasi-parallel and quasi-perpendicular magnetosheath. First, the plasma turbulence is investigated at MHD scales in Section 2 and then at kinetic scales in Section 3. Finally, the results presented are discussed in Section 4, followed by some conclusions.

## 2. MHD-scale Turbulence

In this section, we use fast-mode data from EDP and survey-mode data from FGM and FPI, cadenced at 32, 16, and 0.22 Hz, respectively, and collected in Earth's magnetosheath. To be able to compare the power spectral densities (PSD) of the density and electromagnetic field, the variables are transformed into Alfvén units (see, e.g., Schekochihin et al. 2009; Matteini et al. 2017), as follows:

$$\delta\tilde{n} = \left(1 + \frac{T_i}{T_e}\right)^{1/2} \frac{v_s}{v_A} \left[1 + (v_s/v_A)^2 \left(1 + \frac{T_i}{T_e}\right)\right]^{1/2} \frac{\delta n}{n_0}, \quad (1)$$

$$\delta\tilde{b} = \frac{\delta B}{B_0}, \quad (2)$$

and

$$\delta\tilde{e} = \frac{\delta E}{v_A B_0}, \quad (3)$$

where  $v_A = B_0/\sqrt{\mu_0 n_0 m_i}$  is the Alfvén speed,  $v_s$  is the speed of sound,  $\mu_0$  is the vacuum permeability,  $m_i$  is the ion mass, and  $T_i$  and  $T_e$  are the ion and electron temperatures, respectively.  $B_0$  and  $n_0$  are defined using a low-pass, Finite Impulse Response (FIR) filter (see, e.g., Breuillard et al. 2016) at 0.001 Hz, and spatial and temporal scales are determined, as described in Section 1. We make use of Welch's method (Welch 1967) to compute the PSDs of  $\tilde{b}$ ,  $\tilde{e}$ , and  $\tilde{n}$  in the inertial (MHD) range ( $\sim 0.001$ –0.1 Hz), observed in the quasi-perpendicular (Section 2.1) and quasi-parallel (Section 2.2) magnetosheaths, respectively.

### 2.1. Quasi-perpendicular Magnetosheath

In this section, we use data from MMS1 on 2017 January 2 at 09:00:00–11:00:00 UT, during which it was located in the quasi-perpendicular magnetosheath (see Table 1, case 1). This case corresponds to the slow-mode case ( $v_{bulk}/v_A$ ,  $v_{bulk}/v_{ms} < 1$ ); thus, the Taylor hypothesis may be not valid, and we only show the ion gyrofrequency in Figure 1.

First, we study the slope and the anisotropy (defined here by  $A = \delta B_{parallel}/\delta B_{\perp}$ ) of magnetic-fluctuation spectra, which are divided into perpendicular (dark blue) and parallel (red) components throughout the whole paper, with respect to the mean field,  $B_0$  (defined here by fluctuations below 0.001 Hz).

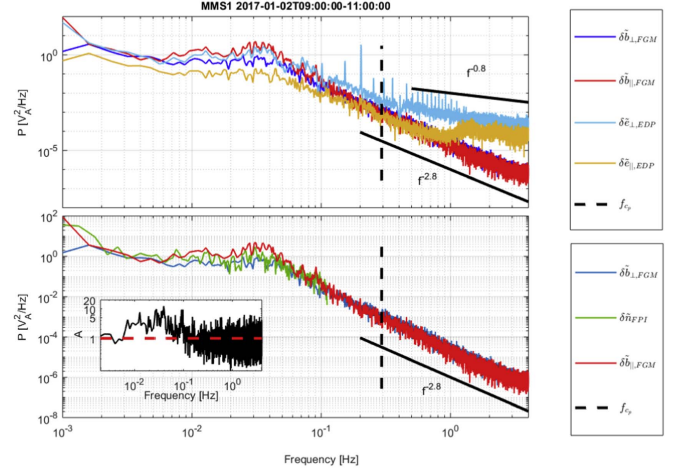


**Figure 1.** Normalized (see Equations (1)–(3)) power spectral densities observed by MMS1 at MHD scales in the quasi-perpendicular MSH during the time interval 09:00–11:00 UT on 2017 January 2. The parallel and perpendicular magnetic-field components measured by FGM are shown in red and dark blue, respectively. The parallel and perpendicular electric-field components measured by EDP are shown in orange and light blue, respectively. The density measured by FPI is displayed in green. The associated black solid line represents the slope of the observed spectra. The vertical dashed line displays the electron gyrofrequency, while the dotted and dashed-dotted lines show the electron gyroradius and inertial length, respectively, estimated using Taylor's hypothesis. The insert shows the anisotropy  $A$  at different frequencies.

Here the assumption of a mean field is accurate, as the fluctuations with frequencies  $>0.001$  Hz are rather weak compared to  $B_0$  ( $\delta B/B_0 \approx 0.1$ ). Figure 1 shows that the fluctuations are anisotropic in the inertial range (0.005–0.1 Hz), with a ratio of  $A \approx 5$ , which is probably due to compressible mirror modes commonly observed at these scales (see, e.g., Schwartz et al. 1996; Sahraoui et al. 2006). However, this anisotropy decreases in the kinetic range ( $f > 0.08$  Hz), as seen in Figure 1 (and detailed in Section 3.1). The electric fluctuations are also anisotropic with  $\delta e_{\perp}/\delta e_{\parallel} \approx 10$ , and this anisotropy also decreases in the kinetic range. The slopes of  $\delta\tilde{e}$  and  $\delta\tilde{b}$  spectra are similar in the inertial range, with an index of  $\alpha \approx -1$ , and show a break at the transition with the kinetic range ( $f_b \approx 0.05$  Hz). In the latter, the spectral index of magnetic fluctuations is approximately  $-2.8$ , whereas the slope of electric fluctuations is shallower (approximately  $-0.8$ , see Figure 1), as expected from theoretical models derived from nonideal terms in Ohm's law (see Section 4).

Then, we investigate the compressible nature of magnetosheath turbulence through the density fluctuations ( $\delta\tilde{n}$ , see above), which are displayed in green in Figure 1. Note that the



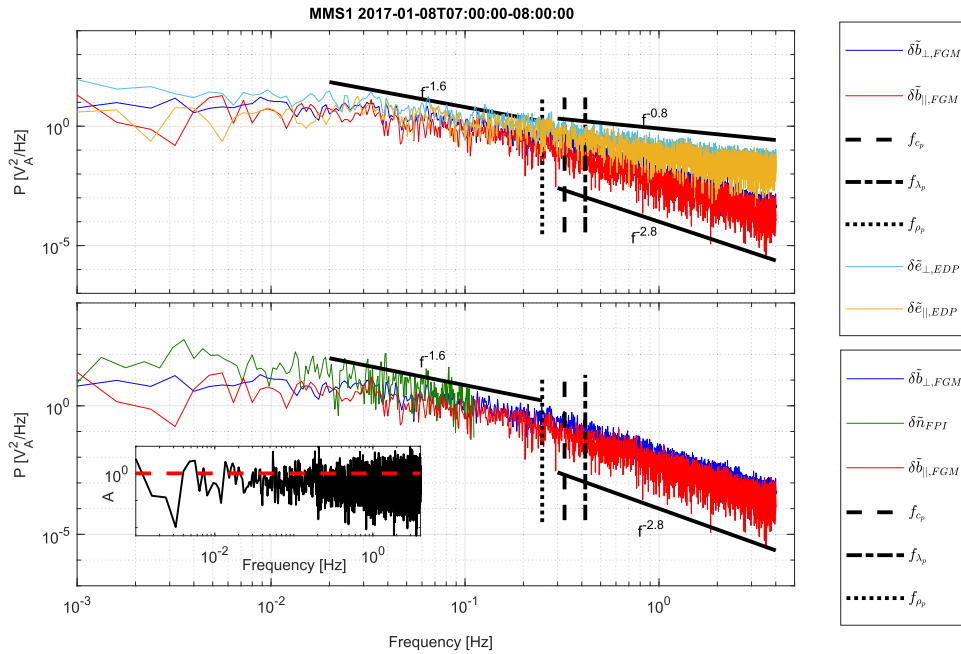


**Figure 2.** Normalized (see Equations (1)–(3)) power spectral densities observed by MMS1 at MHD scales in the quasi-perpendicular MSH during the time interval 07:00–08:00 UT on 2017 January 8. The parallel and perpendicular magnetic-field components measured by FGM are shown in red and dark blue, respectively. The parallel and perpendicular electric-field components measured by EDP are shown in orange and light blue, respectively. The density measured by FPI is displayed in green. The associated black solid lines represent the slope of the observed spectra. The vertical dashed line displays the electron gyrofrequency, while the dotted and dashed–dotted lines show the electron gyroradius and inertial length, respectively, estimated using Taylor’s hypothesis. The insert shows the anisotropy  $A$  at different frequencies.

spectral index is similar to the spectral index of magnetic fluctuations in the inertial range (0.001–0.05 Hz), with a steepening at kinetic scales ( $\alpha \approx -2.8$ ). The amplitude of density fluctuations is also comparable to perpendicular magnetic fluctuations, i.e.,  $\delta\tilde{n}/\delta\tilde{b}_\perp \approx 1$ . We also note here that a higher compressibility (i.e.,  $\delta\tilde{n}/\delta\tilde{b}_\perp > 1$ ) can be found in the flanks of the quasi-perpendicular MSH (not shown).

## 2.2. Quasi-parallel Magnetosheath

Here we use data collected in the quasi-parallel MSH (see Table 1, case 2) by MMS1 on 2017 January 8 at 07:00:00–08:00:00 UT. In this case,  $v_{\text{bulk}}/v_A \approx 2$  and  $v_{\text{bulk}}/v_{\text{ms}} \approx 1.5$ , thus the shift of the frequency spectrum should not be significant (see Section 1) at the scales considered here (i.e., below  $f_{ci}$ ).

In contrast with the quasi-perpendicular MSH, magnetic fluctuations are mostly perpendicular ( $A \approx 0.5$ ) in the inertial range (0.005–0.1 Hz), and the latter increases with increasing frequency. Whereas a spectral index of  $-1$  is observed in the frequency range [0.001–0.02] Hz and  $\alpha \approx -2.8$  in the kinetic range ( $f > 0.3$  Hz), as in a quasi-perpendicular MSH, here an additional power law is observed in between (0.02 and 0.2 Hz) for magnetic fluctuations, with a Kolmogorov-like spectral index of  $\alpha \approx -1.6$ . Nevertheless, one needs to be careful about the anisotropy here since  $\delta B/B_0 \approx 0.25$ , and the assumption of a mean field might not be very accurate. Electric fluctuations are similar to those observed in the quasi-perpendicular MSH, with a steepening of the spectra at the transition with the kinetic range (close to the largest ion scale) and a slope shallower (approximately  $-0.8$ ) than the magnetic spectra (approximately  $-2.8$ ).

In contrast with the quasi-perpendicular MSH, a high compressibility is found downstream of the quasi-parallel

shock in Figure 2, with  $\delta\tilde{n}/\delta\tilde{b}_\perp \approx 10$  in the MHD range. The density spectrum follows the same power law as the  $\delta\tilde{b}_\perp$  in the MHD range, but close to ion scales, it steepens and  $\delta\tilde{n}/\delta\tilde{b}_\perp \approx 1$  at 0.1 Hz. However, the FPI sampling rate in the survey mode is not sufficient to study sub-ion scales; thus, in the following section, we use burst-mode data to study the nature of MSH turbulence in the kinetic range.

## 3. Kinetic-scale Turbulence

In order to study magnetic fluctuations in the sub-ion range, the burst-mode magnetic waveforms from FGM and SCM instruments are merged using an FIR filter (see, e.g., Breuillard et al. 2016), and  $B_0$  and  $n_0$  are defined as low-pass, filtered fluctuations at 0.1 Hz (i.e., below the frequency range of interest). Spatial and temporal scales are again determined as described in Section 1; however, as we will see below, intense whistler turbulence is detected in the quasi-perpendicular MSH, which might violate Taylor’s hypothesis. This is discussed in the next two sections.

### 3.1. Quasi-parallel Magnetosheath

In this case, we have  $v_{\text{bulk}}/v_A > 3$  and  $v_{\text{bulk}}/v_{\text{ms}} > 2$  (see Table 1, case 3), thus the Taylor hypothesis should not be significantly violated, and the frequency shift and flattening of the spectrum should be negligible (see Section 1).

Figure 3 shows that at sub-ion scales (i.e., below the largest electron scale being  $f_{pe}$  here) the anisotropy of magnetic fluctuations is much smaller (here  $A \approx 1$ ) than in the MHD range, as noted in the previous section. Both perpendicular and parallel magnetic spectra follow the classical power law,  $f^{-2.8}$ , which is expected by KAWs and whistler turbulence. In this range, both parallel and perpendicular electric fluctuations

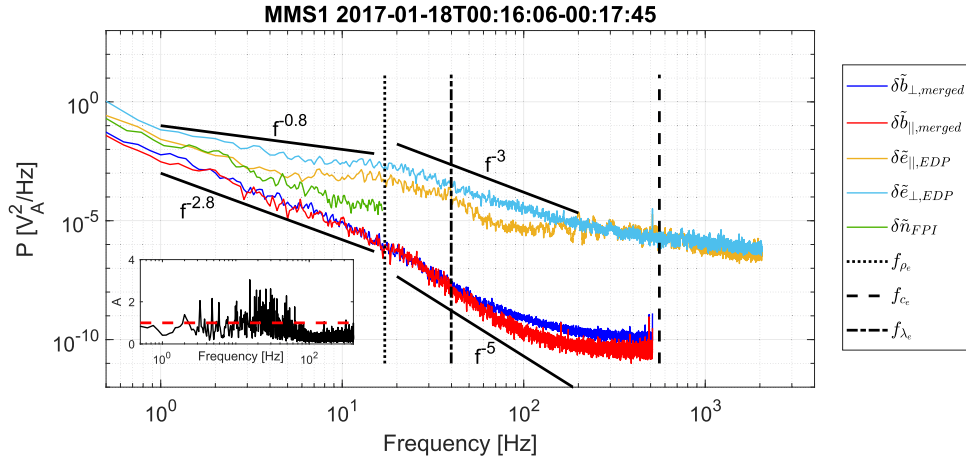


**Figure 3.** Normalized (see Equations (1)–(3)) power spectral densities observed by MMS1 at kinetic scales in the quasi-parallel MSH during the time interval 00:16–00:18 UT on 2017 January 18. The parallel and perpendicular magnetic-field components measured by FGM are shown in red and dark blue, respectively. The parallel and perpendicular electric-field components measured by EDP are shown in orange and light blue, respectively. The density measured by FPI is displayed in green. The associated black solid line represents the slope of the observed spectra. The vertical dashed line displays the electron gyrofrequency, while the dotted and dashed–dotted lines show the electron gyroradius and inertial length, respectively, estimated using Taylor’s hypothesis. The insert shows the anisotropy  $A$  at different frequencies.

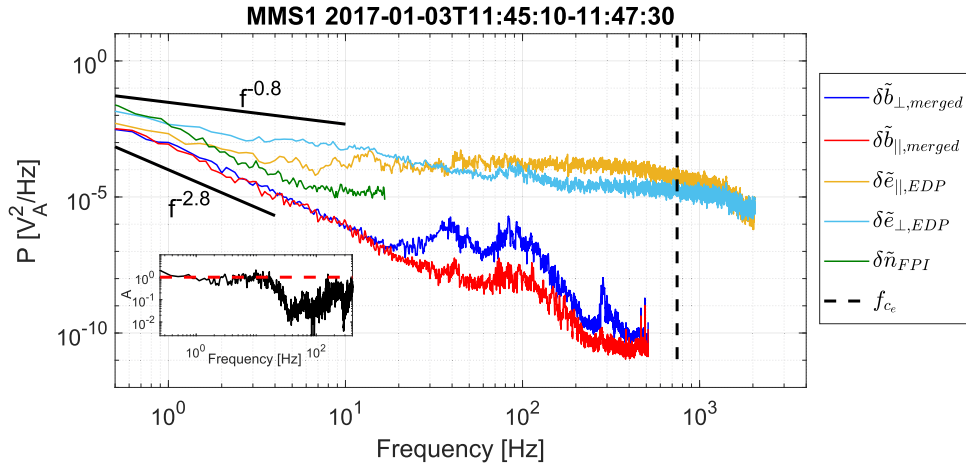


**Figure 4.** Normalized (see Equations (1)–(3)) power spectral densities observed by MMS1 at kinetic scales in the quasi-perpendicular MSH during the time interval 11:45:10–11:47:30 UT on 2017 January 3. The parallel and perpendicular magnetic-field components measured by FGM are shown in red and dark blue, respectively. The parallel and perpendicular electric-field components measured by EDP are shown in orange and light blue, respectively. The density measured by FPI is displayed in green. The associated black solid line represents the slope of the observed spectra. The insert shows the anisotropy  $A$  at different frequencies.

follow an  $f^{-0.8}$  power law, i.e.,  $|\alpha_E| = |\alpha_B| - 2$ , as expected from theoretical models (see Section 4). However, if the density spectrum also roughly follows an  $f^{-2.8}$  power law,  $\delta\tilde{n}/\delta\tilde{b}_\perp \approx 10$ , as in the MHD range, which is not expected from any of the models cited above. We note here that the density spectrum is affected by Poisson noise (for more details, see Gershman et al. 2015) above 10 Hz (not shown) and the flattening of the spectrum is not physical.

At electron scales, i.e., at frequencies above  $f_{\rho_e}$ , magnetic fluctuations are almost isotropic, and their spectra steepen and show a spectral index of  $\alpha \approx -5$  up to  $\sim 100$  Hz. Above that, the magnetic spectrum flattens because SCM reaches its noise floor (not shown), thus measurements are erroneous. At  $f_{\rho_e}$ , the electric fluctuations are more intense than magnetic fluctuations but their anisotropy is high ( $A \approx 5$ ). The electric spectrum also steepens, showing a spectral index of  $\alpha \approx -3 = |\alpha_B| - 2$ , again expected from theoretical models (see Section 4).

However, the electric spectrum flattens close to  $f_{c_e}$  ( $\sim 150$  Hz), whereas EDP does not reach its noise floor, and electric fluctuations may become quasi-isotropic at electron scales.

### 3.2. Quasi-perpendicular Magnetosheath

In this case, we have  $v_{\text{bulk}}/v_A \approx 1.5$  and  $v_{\text{bulk}}/v_{\text{ms}} \approx 1$  (see Table 1, case 4), and as we will see below, intense whistler turbulence is observed, thus the Taylor hypothesis is probably violated at these scales (see Section 1), and we only show the electron gyrofrequency in Figure 4.

Figure 4 shows that at sub-ion scales the anisotropy of magnetic fluctuations is also much smaller (here  $A \approx 1$ ) than in the MHD range. Both perpendicular and parallel magnetic spectra follow the classical power law  $f^{-2.8}$ , which is expected for KAWs and whistler turbulence models. In this range, both parallel and perpendicular electric fluctuations follow an  $f^{-0.8}$  power law, as in the quasi-parallel MSH

and as expected from Hall-MHD models. However, if the density spectrum also roughly follows an  $f^{-2.8}$  power law,  $\delta\tilde{n}/\delta\tilde{b}_\perp \approx 10$  as in quasi-parallel MSH. We note here that although  $\delta\tilde{n}/\delta\tilde{b}_\perp \approx 1$  is usually observed in the quasi-perpendicular MSH (see Figure 1),  $\delta\tilde{n}/\delta\tilde{b}_\perp \gg 1$  can occur when the solar wind flow pressure is high enough ( $>5\text{--}6$  nPa, see Table 1).

Between ion and electron scales, magnetic fluctuations are almost isotropic and the spectra steepen at  $\sim 10$  Hz. However, large quasi-perpendicular fluctuations (identified as whistlers by polarization analysis, not shown) observed in the range [20–400] Hz (i.e.,  $0.025 - 0.5f_{ce}$  here) form large bumps in the perpendicular magnetic spectrum. They also form smaller bumps in the parallel magnetic component, thus in the perpendicular electric component. Although the latter globally steepens at these scales, the parallel electric component seems to flatten at  $\sim 40$  Hz and dominates ( $\tilde{e}_\parallel/\tilde{e}_\perp \approx 10$ ) from  $\sim 100$  Hz up to  $\sim 1600$  Hz (i.e.,  $2f_{ce}$ ). Thus the fluctuations may become quasi-electrostatic and parallel to the magnetic field above the whistler frequency range, i.e., ( $0.2f_{ce}$ ). Above, the electric spectra seem to steepen again, but at these frequencies, SCM reaches its noise floor and the magnetic spectra are not reliable.

#### 4. Discussion and Conclusions

In this study, we make use of the high-time sampling rate (burst-type data) of the *MMS* mission to investigate the nature of turbulence in Earth’s magnetosheath with respect to the angle between the interplanetary magnetic field and the shock normal. In this section, we discuss the results obtained and their implications.

We show a new type of highly compressible turbulence in the MSH, with a typical ratio  $\delta\tilde{n}/\delta\tilde{b}_\perp \approx 5\text{--}10$  (see also Hadid 2016). This is in contrast with what is usually observed in the solar wind, where  $\delta\tilde{n}/\delta\tilde{b}_\perp \approx 0.1\text{--}0.75$ , except in rare cases (see Chen et al. 2013). This ratio is rather constant up to sub-ion scales, i.e., the compressibility is transferred toward kinetic scales. We find that it is observed in the quasi-parallel MSH for all selected time intervals and in the quasi-perpendicular MSH when the solar wind flow pressure is high enough ( $>5$  nPa). Therefore, this turbulence might be composed of coherent structures superimposed on an Alfvénic-type turbulence. Recent studies of turbulence models, including compressibility, have shown that at MHD scales compressibility increases the heating rate in the solar wind (Hadid et al. 2017) and in the magnetosheath (Hadid et al. 2018). However, such models at sub-ion scales are still in development (e.g., Andrés et al. 2018), and the comparison with observations is left for future studies.

We also show that an inertial range, i.e., a Kolmogorov-like spectrum (with  $\alpha \approx -5/3$ ) between MHD and sub-ion scales, is found in the subsolar quasi-parallel MSH, as it is usually found in the flanks (Alexandrova et al. 2008; Huang et al. 2017), but not downstream of the quasi-perpendicular BS (as previously noted by Shevryev et al. 2006). This developed turbulence (i.e., the time of travel is longer than the eddy turnover time) suggests that the turbulent fluctuations are created upstream of the MSH (i.e., at or upstream of the BS) in the quasi-parallel MSH, whereas they are created locally in the quasi-perpendicular MSH.

We also note here that the magnetic fluctuations are found to be more anisotropic at MHD scales than at kinetic scales (which is in agreement with what has been found behind a quasi-parallel shock (see, e.g., Perri et al. 2009)), except when intense waves are locally observed (e.g., the whistlers in Figure 4). Moreover, we show that the spectral break, which

shows the transition from the MHD (or inertial range) to the kinetic regime, occurs at a frequency close to the largest ion scale (here  $f_{\rho_p}$ ) in the quasi-perpendicular and quasi-parallel MSH, as already stated in Breuillard et al. (2016) using measurements from the Cluster mission.

At sub-ion scales, the magnetic and electric fluctuations become more isotropic and follow  $f^{-2.8}$  and  $f^{-0.8}$  power laws, respectively. The spectra steepen close to electron scales and, in the absence of kinetic waves (e.g., whistlers, see Figure 3), the spectral index of magnetic fluctuations becomes  $\alpha \approx -5$ , as predicted for KAW turbulence ( $\alpha \approx -16/3$ ) at the sub-Larmor scale (Schekochihin et al. 2009). As to the spectral index of electric fluctuations, it is observed to be approximately  $-3$ . Therefore, at kinetic scales,  $E_E \propto k^2 E_B$ , as predicted by theoretical models derived from the nonideal terms in Ohm’s law (see Sahraoui et al. 2009; Franci et al. 2018, and references therein) and observed on Cluster (Huang et al. 2014; Matteini et al. 2017). This is consistent with the fact that the slope of density fluctuations is the same as magnetic fluctuations at sub-ion scales, as observed in Figures 3 and 4 (see also Chen & Boldyrev 2017).

We note here that in Figure 3 the steepening of the spectra occurs at the largest-electron scale (i.e., with the lowest frequency), like the spectral break at ion scales (see Breuillard et al. 2016). However, it is difficult to determine statistically at which electron scale the steepening occurs since whistler waves are often observed at these frequencies, notably in the quasi-perpendicular MSH (see Figure 4), which can violate the Taylor hypothesis (see, e.g., Klein et al. 2014).

Finally, we show that the magnetosheath turbulence is dominated, to a great extent, by electric-field fluctuations at electron scales, i.e., at frequencies  $\sim 100$  Hz. This can have broad implications for the understanding of energy dissipation at these scales, notably for kinetic turbulence models. However, this question is beyond the scope of the present article.

Above 100 Hz, the electric fluctuations are quasi-isotropic when no waves are observed (see Figure 3). However, they seem to be mostly parallel ( $\delta\tilde{e}_\parallel/\delta\tilde{e}_\perp \approx 10$ ) at electron scales and beyond, i.e., in the range  $[0.2\text{--}2] f_{ce}$ , when whistlers are observed (see Figure 4). This result would suggest that energy dissipation, heating, and acceleration in the quasi-perpendicular MSH might be driven by intense electrostatic parallel structures/waves, such as electrostatic solitary waves (identified here, but not shown), which can be linked to whistler waves (see, e.g., Wilder et al. 2016). However, to confirm these speculations, a detailed study of these electric fluctuations is required and left for future work.

H.B.’s work has been supported by the CNES grant “Allocations de recherche post-doctorale.”

#### ORCID iDs

L. Matteini  <https://orcid.org/0000-0002-6276-7771>  
M. R. Argall  <https://orcid.org/0000-0001-6315-1613>  
A. Vaivads  <https://orcid.org/0000-0003-1654-841X>  
Yu. V. Khotyaintsev  <https://orcid.org/0000-0001-5550-3113>  
A. Chasapis  <https://orcid.org/0000-0001-8478-5797>

#### References

- Alexandrova, O., Chen, C. H. K., Sorriso-Valvo, L., Horbury, T. S., & Bale, S. D. 2013, *SSRv*, **178**, 101  
Alexandrova, O., Lacombe, C., & Mangeney, A. 2008, *AnGeo*, **26**, 3585

- Alexandrova, O., Lacombe, C., Mangeney, A., Grappin, R., & Maksimovic, M. 2012, [ApJ](#), **760**, 121
- Alexandrova, O., Saur, J., Lacombe, C., et al. 2009, [PhRvL](#), **103**, 165003
- Andrés, N., Galtier, S., & Sahraoui, F. 2018, [PhRvE](#), **97**, 013204
- Bale, S. D., Kasper, J. C., Howes, G. G., et al. 2009, [PhRvL](#), **103**, 211101
- Breuillard, H., Yordanova, E., Vaivads, A., & Alexandrova, O. 2016, [ApJ](#), **829**, 54
- Bruno, R., & Carbone, V. 2013, [LRSP](#), **10**, 2
- Chen, C. H. K., & Boldyrev, S. 2017, [ApJ](#), **842**, 122
- Chen, C. H. K., Boldyrev, S., Xia, Q., & Perez, J. C. 2013, [PhRvL](#), **110**, 225002
- Czaykowska, A., Bauer, T. M., Treumann, R. A., & Baumjohann, W. 2001, [AnGeo](#), **19**, 275
- Ergun, R. E., Tucker, S., Westfall, J., et al. 2016, [SSRv](#), **199**, 167
- Fairfield, D. H., & Ness, N. F. 1970, [JGR](#), **75**, 6050
- Franci, L., Cerri, S. S., Califano, F., et al. 2017, [ApJL](#), **850**, L16
- Franci, L., Landi, S., Matteini, L., Verdini, A., & Hellinger, P. 2016, [ApJ](#), **833**, 91
- Franci, L., Landi, S., Verdini, A., Matteini, L., & Hellinger, P. 2018, [ApJ](#), **853**, 26
- Fuselier, S. A., Lewis, W. S., Schiff, C., et al. 2016, [SSRv](#), **199**, 77
- Gershman, D. J., Dorelli, J. C., F.-Viñas, A., & Pollock, C. J. 2015, [JGRA](#), **120**, 6633
- Hadid, L. Z. 2016, PhD thesis, Université Paris-Saclay
- Hadid, L. Z., Sahraoui, F., & Galtier, S. 2017, [ApJ](#), **838**, 9
- Hadid, L. Z., Sahraoui, F., Galtier, S., & Huang, S. Y. 2018, [PhRvL](#), **120**, 055102
- Howes, G. G., Klein, K. G., & TenBarge, J. M. 2014, [ApJ](#), **789**, 106
- Huang, S. Y., Du, J. W., Sahraoui, F., et al. 2017a, [JGRA](#), **122**, 8577
- Huang, S. Y., Hadid, L. Z., Sahraoui, F., Yuan, Z. G., & Deng, X. H. 2017, [ApJL](#), **836**, L10
- Huang, S. Y., Sahraoui, F., Deng, X. H., et al. 2014, [ApJL](#), **789**, L28
- Huang, S. Y., Sahraoui, F., Yuan, Z. G., et al. 2017b, [ApJL](#), **836**, L27
- Iroshnikov, P. S. 1963, [AZh](#), **40**, 742
- Klein, K. G., Howes, G. G., & TenBarge, J. M. 2014, [ApJL](#), **790**, L20
- Kraichnan, R. H. 1965, [PhFl](#), **8**, 1385
- Le Contel, O., Leroy, P., Roux, A., et al. 2016, [SSRv](#), **199**, 257
- Le, G., & Russell, C. T. 1992, [P&SS](#), **40**, 1215
- Lindqvist, P.-A., Olsson, G., Torbert, R. B., et al. 2016, [SSRv](#), **199**, 137
- Matteini, L., Alexandrova, O., Chen, C. H. K., & Lacombe, C. 2017, [MNRAS](#), **466**, 945
- Perri, S., Yordanova, E., Carbone, V., et al. 2009, [JGRA](#), **114**, a02102
- Pollock, C., Moore, T., Jacques, A., et al. 2016, [SSRv](#), **199**, 331
- Russell, C. T., Anderson, B. J., Baumjohann, W., et al. 2016, [SSRv](#), **199**, 189
- Russell, C. T., & Farris, M. H. 1995, [AdSpR](#), **15**, 285
- Sahraoui, F., Belmont, G., Rezeau, L., et al. 2006, [PhRvL](#), **96**, 075002
- Sahraoui, F., Goldstein, M. L., Robert, P., & Khotyaintsev, Y. V. 2009, [PhRvL](#), **102**, 231102
- Schekochihin, A. A., Cowley, S. C., Dorland, W., et al. 2009, [ApJS](#), **182**, 310
- Schwartz, S. J., Burgess, D., & Moses, J. J. 1996, [AnGeo](#), **14**, 1134
- Sekopke, N., Paschmann, G., Bame, S. J., Gosling, J. T., & Russell, C. T. 1983, [JGR](#), **88**, 6121
- Shevryev, N. N., Zastenker, G. N., Eiges, P. E., & Richardson, J. D. 2006, [AdSpR](#), **37**, 1516
- Shue, J.-H., Song, P., Russell, C. T., et al. 1998, [JGRA](#), **103**, 17691
- Taylor, G. I. 1938, [RSPSA](#), **164**, 476
- Thomsen, M. F., Gosling, J. T., Bame, S. J., & Russell, C. T. 1985, [JGR](#), **90**, 267
- Welch, P. 1967, [IEEE Transactions on Audio and Electroacoustics](#), **15**, 70
- Wilder, F. D., Ergun, R. E., Goodrich, K. A., et al. 2016, [GeoRL](#), **43**, 5909
- Zimbaro, G., Greco, A., Sorriso-Valvo, L., et al. 2010, [SSRv](#), **156**, 89